



# CHORUS

This is the accepted manuscript made available via CHORUS. The article has been published as:

## Local Quantum Criticality of an Iron-Pnictide Tetrahedron

T. Tzen Ong and Piers Coleman

Phys. Rev. Lett. **108**, 107201 — Published 5 March 2012

DOI: [10.1103/PhysRevLett.108.107201](https://doi.org/10.1103/PhysRevLett.108.107201)

# Local Quantum Criticality of an Iron-Pnictide Tetrahedron

T. Tzen Ong<sup>1</sup> and Piers Coleman<sup>1,2</sup>

<sup>1</sup>Center for Materials Theory, Department of Physics & Astronomy, Rutgers University, Piscataway NJ 08854, USA

<sup>2</sup>Department of Physics, Royal Holloway, University of London, Egham, Surrey TW20 0EX, UK

(Dated: December 19, 2011)

Motivated by the close correlation between transition temperature ( $T_c$ ) and the tetrahedral bond angle of the As-Fe-As layer observed in the iron-based superconductors, we study the interplay between spin and orbital physics of an isolated iron-arsenide tetrahedron embedded in a metallic environment. Whereas the spin Kondo effect is suppressed to low temperatures by Hund's coupling, the orbital degrees of freedom are expected to quantum mechanically quench at high temperatures, giving rise to an overscreened, non-Fermi liquid ground-state. Translated into a dense environment, this critical state may play an important role in the superconductivity of these materials.

The discovery of superconductivity with  $T_c = 26\text{K}$  in LaFeAsO by Hosono *et. al.* [1] has opened up a new field of iron-based high temperature superconductors (SCs). Experimental studies suggest a range of electron correlation effects. For example, in the undoped parent antiferromagnets, neutron scattering studies show a small ordered moment in the pnictides, but a significantly larger moment in the chalcogenides[2]. Similarly, optical studies in  $BaFe_2As_2$  and  $SrFe_2As_2$  indicate a spin-density wave (SDW) gap [3] normally associated with itinerant electrons while optical studies in LaFePO [4] and ARPES results in  $FeSe_{0.42}Te_{0.58}$  [5, 6] suggest significant correlation effects. This diversity of behavior has prompted an active debate on the role of electron correlation effects. While some groups favor a more localized theoretical description[7, 8], many theoretical treatments[9] have favored an itinerant, multi-band description.

One aspect of these systems that is poorly understood, concerns the strong connection between the many body physics and solid-state chemistry[10]. In these superconductors the iron atom sits inside a tetrahedral cage of pnictide (As,P) or chalcogenide (Te,Se) atoms. Experiments show that the transition temperature is maximal when the bond-angles most closely approximate a perfect tetrahedron ( $\theta(\text{As-Fe-As}) = 109.5^\circ$ )[11, 12]. More recent studies[13] show that c-axis compression of the tetrahedra causes the superconducting gap to become anisotropic, ultimately developing line nodes[14].

Motivated by these issues, here we develop a theory for an isolated iron-tetrahedron embedded within a conduction sea. One of our key observations, is that in addition to their spin physics, the iron-based tetrahedra develop an orbital degree of freedom associated with the degenerate  $e_g$  orbitals. For conventional transition metal ions, the Hund's coupling  $J_H$  locks the unpaired electrons together into a high spin configuration, exponentially suppressing the spin-Kondo temperature to low temperatures according to an effect discovered by Schrieffer [15]. Here we show that unlike their spin counterparts, orbital fluctuations are not subject to the ‘‘Schrieffer effect’’, giving rise to a unique situation in which the orbital degrees of freedom behave as fluctuating quan-

tum mechanical variables that result in an incoherent ‘‘non-Fermi liquid’’ ground-state. While departures from perfect tetragonality will re-establish the Fermi liquid, a large temperature range of incoherent metal behavior is expected to remain.

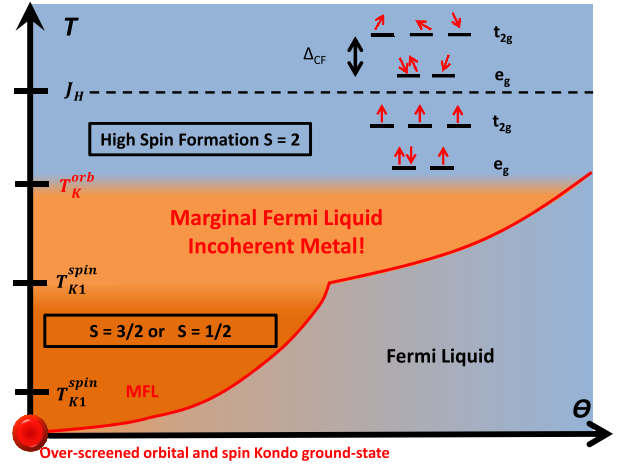


FIG. 1. Phase diagram of single Fe in an As tetrahedron. At  $T \sim J_H$ , the Hund's coupling locks the spins of the Fe atom into an  $S = 2$  state, and the orbital Kondo effect flows to strong coupling, giving rise to a Marginal Fermi Liquid overscreened state at  $T \sim T_K^{orbital}$ . The dangerously irrelevant spin Kondo interaction finally drives the system to an overscreened spin Kondo ground state at  $T_{K2}^{spin}$ .  $\theta$  is the deviation away from perfect tetrahedral symmetry, where  $\theta_c = 109.5^\circ$ , and will break the  $SU(2)^{orb}$  symmetry and restore Fermi liquid behavior.

We assume that the FeAs tetrahedron contains an  $Fe^{2+}$  ion in an  $3d^6$  configuration. In a tetrahedral environment, the five  $d$ -electron orbitals are split by the crystal field  $\Delta_{CF}$  into three degenerate upper  $t_{2g}$  orbitals and the two degenerate lower  $e_g$  orbitals, as shown in Fig. 2. When the tetrahedron is perfect, the unpaired electron in the lower  $e_g$  orbitals can sit in the  $d_{3z^2-r^2}$  or the  $d_{x^2-y^2}$  orbital, giving rise to an unquenched orbital degree of freedom. Using a perturbative renormalization group treatment, we show that at high energies, orbital

Kondo fluctuations dominate and the system flows to an over-screened orbital Kondo fixed point. The residual low energy orbital degrees of freedom condense into a single Majorana fermion that scatters electrons to produce a Marginal Fermi liquid (MFL). By analyzing the physics of this state using a strong coupling expansion, we show that the subsequent low temperature spin Kondo effect is also overscreened, so that the the FeAs tetrahedron is a critical system down to the lowest temperatures.

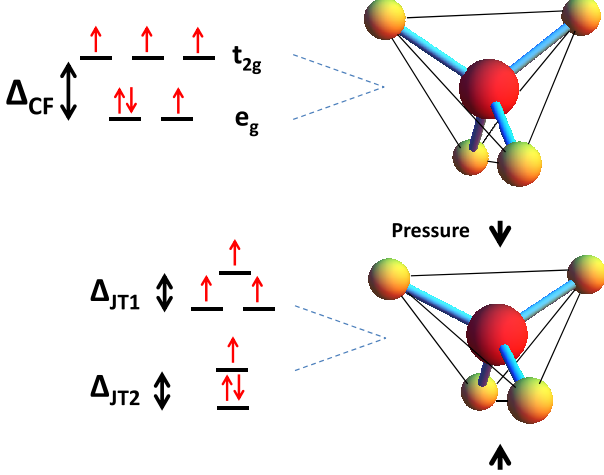


FIG. 2. Crystal field splitting of the  $d$ -electron orbitals in a tetrahedron into the upper  $t_{2g}$  and lower  $e_g$  orbitals. The lower diagram shows effect of compression along the  $c$ -axis, which lifts the two-fold degeneracy in the  $e_g$  orbitals.

The local physics of a single FeAs tetrahedron can be modeled by an Anderson model  $H = H_0 + H_A$  that describes the hybridization of Hund’s coupled  $d$ -electrons in five electron channels  $\Gamma \in [t_{2g}, e_g]$ , where

$$\begin{aligned}
 H_0 &= \sum_{\vec{k}\sigma\Gamma} \epsilon_{\vec{k}} c_{\vec{k}\Gamma\sigma}^\dagger c_{\vec{k}\Gamma\sigma}, \\
 H_A &= \sum_{\Gamma \in [t_{2g}, e_g]} (V_\Gamma d_{\Gamma\sigma}^\dagger \psi_{\Gamma\sigma} + \text{H.c.}) + \epsilon_\Gamma d_{\Gamma\sigma}^\dagger d_{\Gamma\sigma} \\
 &+ \sum_{\Gamma \in [t_{2g}, e_g]} +U n_{\Gamma\sigma} n_{\Gamma\bar{\sigma}} - J_H |\vec{S}|^2
 \end{aligned} \quad (1)$$

Here,  $\vec{S} = 1/2 \sum_\Gamma d_{\Gamma\alpha}^\dagger \vec{\sigma}_{\alpha\beta} d_{\Gamma\beta}$ , is the total spin of the  $d$ -electrons,  $\epsilon_\Gamma$  the energy of the crystal field level  $\Gamma$ , while  $\psi_{\Gamma\alpha}^\dagger = \sum_{\vec{k}} c_{\vec{k}\Gamma\alpha}^\dagger$  creates a conduction electron at the origin in channel  $\Gamma$ . We shall assume that the Hubbard interaction,  $U$ , is the largest scale in the problem, with a hierarchy of energy scales given by  $U > D > J_H > V_\Gamma$ , where  $D$  is the electron bandwidth.

The effective low energy Hamiltonian,  $H = H_0 + H_K$ , can be derived by a Schrieffer-Wolff transformation.

$$\begin{aligned}
 H_K &= \frac{J_2}{4S} \vec{S} \cdot \vec{\sigma}_{t_{2g}}(0) \\
 &+ J \left( \frac{1}{2S} \vec{S} \cdot \vec{\sigma}_{e_g}(0) + \frac{1}{2} \mathbb{1} \right) \left( \vec{T} \cdot \vec{\tau}(0) + \frac{1}{2} \mathbb{1} \right)
 \end{aligned} \quad (2)$$

with the Kondo coupling in each channel given by  $J_\Gamma = 2|V_\Gamma|^2(1/|\epsilon_\Gamma| + 1/(U + \epsilon_\Gamma))$ , and  $J = J_{t_{2g}}$ ,  $J_2 = J_{e_g}$ ;  $\vec{\sigma}_\Gamma(0) = \frac{1}{2} \psi_{\Gamma\alpha}^\dagger \vec{\sigma}_{\alpha\beta} \psi_{\Gamma\beta}$  is the conduction electron spin-density at the origin in channel  $\Gamma$ , while  $\vec{\tau}(0) = \frac{1}{2} \sum_{\Gamma\Gamma' \in e_g} \psi_{\Gamma\alpha}^\dagger \vec{\tau}_{\Gamma\Gamma'} \psi_{\Gamma'\alpha}$  is the orbital moment of the conduction electrons in the  $e_g$  channel. This model is isotropic in orbital space; the layered structure of real iron-based materials will break the Heisenberg orbital symmetry, however these departures from isotropy will scale to zero as a result of the orbital Kondo effect.

The first term in  $H_K$  describes the Kondo interaction in the  $t_{2g}$  orbitals, while the second term, reminiscent of a local “Kugel Khomskii” interaction[22, 23], describes the mixing of  $e_g$  spin and orbital degrees of freedom: for  $S = 1/2$ , this is the well-known SU(4) Kondo interaction, but for large Hund’s coupling, the system is locked into a high spin state with  $S = 2$ . Projected into this subspace, the interaction in the  $e_g$  orbitals factorizes into spin and orbital Kondo interactions.

One of the effects of the projection into the high-spin manifold is an  $S$ -fold reduction of the spin Kondo coupling,  $J_S = J/4S$  but strikingly, the strength of the orbital Kondo interaction is unaffected. This means that the Hund’s interaction will exponentially suppress the spin Kondo effect down to a lower scale  $T_K^{spin}/D \sim (T_K^{orb}/D)^{2S}$ , as in conventional transition metal ions, while leaving the orbital Kondo effect unaffected. This schism between the orbital and spin Kondo effect drastically affects the physics, as we now confirm from a renormalization analysis.

A perturbative RG treatment of Eq. 2 is carried out, with the Feynman diagrams shown in Fig. 3; and the dimensionless coupling constants are defined as  $g_S = \frac{J}{4S} \rho(E_F)$ ,  $g_T = \frac{J}{2} \rho(E_F)$  and  $g_m = \frac{J}{2S} \rho(E_F)$ . Since there are no orbital fluctuations in the  $t_{2g}$  orbitals, we just obtain the standard Kondo result for  $J_2$ . In the  $e_g$  channels, there are contributions to  $\beta_{g_S}$  and  $\beta_{g_T}$  from the “mixed” Kondo term, which are proportional to  $|\vec{T}|^2 g_m^2$  and  $|\vec{S}|^2 g_m^2$  respectively. Hence, the beta-functions are,

$$\begin{aligned}
 \beta_{g_T} &= -2g_T^2 - 2S(S+1)g_m^2 \\
 \beta_{g_S} &= -2g_S^2 - \frac{3}{2}g_m^2 \\
 \beta_{g_m} &= 8g_m^2 - 4g_m g_T - 4g_m g_S
 \end{aligned} \quad (3)$$

Since both  $g_S$  and  $g_m$  are of order  $O(1/S)$ , while  $g_T$  is of order  $O(1)$ , clearly  $\beta_{g_T}$  is of order  $O(1)$  and  $\beta_{g_m} \sim O(1/S)$  and  $\beta_{g_S} \sim O(1/S^2)$ . Hence,  $g_T$  is the most relevant perturbation, and the system initially flows towards the over-screened orbital fixed point at  $T = T_K^{orb}$ . The key result is that the quenching of the orbital degrees of freedom leaves behind an unscreened  $S = 2$  spin moment, coupled to five independent screening channels. While orbital fluctuations are quenched below  $T_K^{orb}$ , we might expect that only remaining local degrees of freedom would be the local  $S = 2$  spin, Kondo coupled to

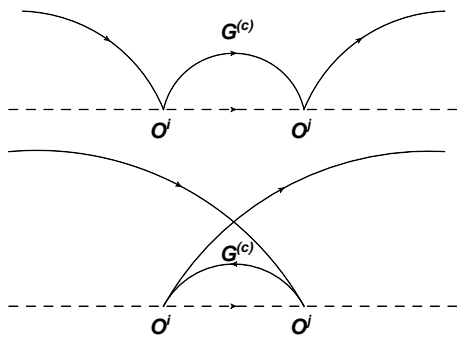


FIG. 3. The two one loop diagrams that contribute to the renormalization of  $g_T$ ,  $g_S$  and  $g_m$ . Here, the operator  $O$  corresponds to the spin, iso-spin or “mixed” Kondo operator, i.e.  $\vec{O} \in [\vec{\sigma}, \vec{\tau}, \vec{\sigma}\vec{\tau}]$ , and the dashed line corresponds to the local conduction electron propagator  $G^{(c)}(\omega)$ .

the five channels. From this point-of-view, the effective Hamiltonian will be an overscreened five-channel  $S = 2$  Kondo model consisting of the first two terms in Eq. 4.

$$H = H_0 + \sum_{\Gamma} J_{\Gamma} \vec{S} \cdot \psi_{\Gamma\alpha}^{\dagger} \frac{\vec{\sigma}_{\alpha\alpha'}}{2} \psi_{\Gamma\alpha'} + H_{res} \quad (4)$$

However, this reasoning ignores certain subtle low-energy excitations generated by the orbital Kondo effect, that we have anticipated by including a further term  $H_{res}$ . In fact, the orbital Kondo effect couples to the spin up and spin down conduction electrons, and is thus overscreened. This gives rise to a well-documented MFL state with a zero-energy excitation described by a single Majorana fermion  $\phi(0)$  [17–19]. The interaction with the spin and conduction electrons must be taken into account. This requires decoupling the spin and orbital sectors of the  $e_g$  conduction electrons in terms of itinerant Majorana fermions,  $(\psi^0, \vec{\psi})$ , and  $(\chi^0, \vec{\chi})$ , which respectively carry the spin and orbital quantum numbers.

In the strong-coupling limit, the Hamiltonian is projected into the degenerate orbital singlets subspace. Clearly, the spin Kondo term depends only on the  $\psi$  fermions that carry spin, whereas the mixed Kondo term depends on both  $\psi$  and  $\chi$  fermions as it can mix the two singlet states. The Majorana fermion at the origin,  $\phi(0) = \chi^1(0)\chi^2(0)\chi^3(0)$  is a three-fermion composite, and it couples to the  $\chi$  fermions at the neighboring site via the kinetic term; thus the first non-trivial term is  $3^{\text{rd}}$ -order,  $\alpha = 3t^3/4g_T^2$ . The effective strong coupling Hamiltonian,  $\tilde{H}$ , is therefore,

$$\begin{aligned} \tilde{H} = & it \sum_{n=1}^{n=\infty} \sum_{a=0}^3 [\psi^a(n+1)\psi^a(n) + \chi^a(n+1)\chi^a(n)] \\ & + \alpha\phi(0)\chi^1(1)\chi^2(1)\chi^3(1) - i\frac{g_S}{2}\vec{S} \cdot (\vec{\psi}(0) \times \vec{\psi}(0)) \\ & + \frac{g_m}{2}\psi^0(0)\vec{S} \cdot \vec{\psi}(0)\phi(0)\chi^0(0) + H_{0,t_{2g}} + H_{K,t_{2g}} \end{aligned} \quad (5)$$

where  $H_{0,t_{2g}}$  and  $H_{K,t_{2g}}$  are the kinetic energy of the conduction electrons and the Kondo interaction in the  $t_{2g}$  channel. Dimensional analysis shows that the canonical dimensions of the Majorana fermions and coupling constants are  $[\psi]_L = [\chi]_L = -\frac{1}{2}$ ,  $[g_S]_L = 0$  and  $[g_m]_L = \frac{1}{2}$  so  $g_m$  is irrelevant around the strong coupling fixed point.

We then carried out a one loop calculation of the renormalization of  $g_S$ . At  $T = 0$ , the local Majorana fermions propagators  $G^{\chi}(\tau) = G^{\psi}(\tau) \sim \frac{1}{\tau}$ , and  $G^{\phi}(\tau) = \frac{1}{2}\text{sgn}(\tau)$ , which means that at one loop order, there is a  $(g_S/2)^2 \ln\Lambda$  correction to  $g_S$ , where  $\Lambda$  is an UV cut-off, whereas  $g_m$  does not contribute. This shows that the spin Kondo coupling,  $g_S$ , is marginally relevant around the strong coupling fixed point, and will finally drive the system into an over-screened spin and orbital Kondo ground state with a different MFL. Therefore, the system is a quantum-critical incoherent metal down to 0 K.

Fig. 4 shows the renormalization flows for the system. The perfectly-screened Fermi liquid fixed point lies in plane I, defined by  $\beta_{g_m} = 0$ , along the line  $\beta_{g_T} = \alpha(S)g_S$ . For  $S = 1/2$ ,  $\alpha(S) = 1$  and we recover the  $SU(4)$  Fermi liquid fixed point, which is characterized by perfect screening of the spin and orbital degrees of freedom.

The FeAs tetrahedron initially flows towards the over-screened orbital Kondo fixed point, where orbital fluctuations are quenched at  $T_K^{orb}$ . It will then cross-over to an over-screened orbital and spin Kondo fixed point at a lower temperature  $T_K^{spin}$ , and two different MFLs arise at  $T_K^{orb}$  and  $T_K^{spin}$  due to over-screened orbital and spin Kondo physics respectively. The over-screened spin Kondo fixed point with  $n$  channels lies at  $g^* = \frac{2}{n}(1 - \frac{2}{n} \ln 2)$  [20]; hence, the over-screened orbital and spin fixed point lies on the line  $g_T \approx \frac{n_s}{n_o} g_S \approx 5/2 g_S$ .

Fig. 1 summarizes the phases, and the Fe impurity forms an  $S = 2$  local moment at a temperature  $T \sim J_H$ . Due to the Schrieffer mechanism for Kondo resonance narrowing, the orbital and spin Kondo temperatures are split,  $(T_K^{orb}/D)^{2S} \sim T_K^{spin}/D$ , and for  $T_K^{orb} < T < T_K^{spin}$ , the system flows towards a two channel orbital Kondo fixed point with MFL behavior.

At temperatures below  $T_K^{orb}$ , the orbital fluctuations in the  $e_g$  orbitals are quenched leaving an  $S = 2$  spin interacting with five channels of conduction electrons. The system will first be screened from an  $S = 2$  state to an  $S = \frac{1}{2}$  or  $S = 1$  state, depending on the relative strengths of the  $t_{2g}$  and  $e_g$  Kondo couplings; and will finally be completely screened at a lower temperature  $T_K^{spin}$ . It is possible that these two scenarios could correspond to the chalcogenides and pnictides respectively.

In practice, real systems deviate from perfect tetrahedral symmetry, and breaking of the  $SU(2)^{\text{orbital}}$  symmetry would lift the  $e_g$  orbitals degeneracy via a Jahn-Teller splitting  $\Delta_{JT}$ . It is well known from two channel Kondo physics that this will restore Fermi liquid behavior below an energy scale  $\Delta_{JT}^2/T_K^{orb}$ . This Fermi liquid behavior

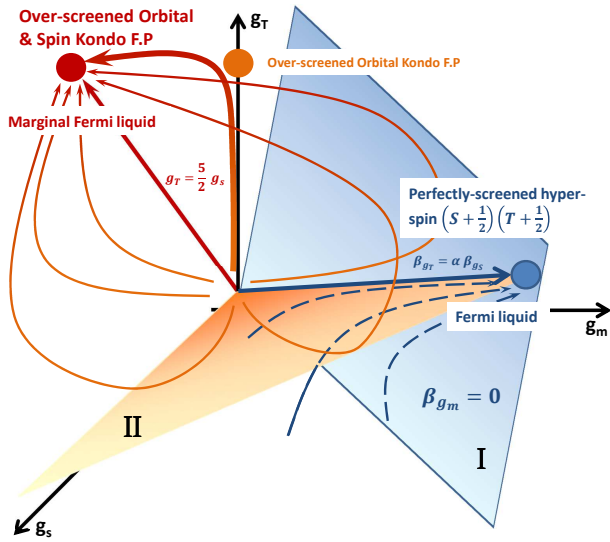


FIG. 4. Schematic plot of the RG flow. The perfectly screened hyper-spin Fermi liquid fixed point lies along the line  $\beta_{g_T} = \alpha(S)g_s$  in plane I, and is stable against weak breaking of SU(4) symmetry [23]. For strong asymmetry, the system flows to the over-screened orbital and spin Kondo Marginal Fermi Liquid fixed point. The blue plane I is defined by  $\beta_{g_m} = 0$ , and the orange plane II is defined by  $\beta_{g_T} = \alpha(g_m, S)\beta_{g_s}$ . The bold line indicates the expected RG flow for a realistic FeAs tetrahedron.

will be seen only if  $\Delta_{JT}^2/T_K^{orb} > T_{K1}^{spin}$ . Raman spectroscopy indicates  $\Delta_{JT} \sim 20-30$  meV [21], and  $T_K \sim 0.1$  eV for some transition metals[24]. In general, we expect  $T_K^{orb} > \Delta_{JT}$ , meaning that the large  $T_K^{orb}$  will protect the system against breaking of the tetrahedral symmetry, thus preserving the critical over-screened phases for a range of applied pressures in experiments.

Various aspects of our theory could be tested in dilution experiments on materials such as  $Ba(Ru_{1-x}Fe_xAs)_2$ . The presence of local moment behavior is expected to give rise to a Kondo resistance minimum. Our theory also predicts a logarithmic temperature dependence of the orbital susceptibility,  $\chi_o \sim \ln T$  below  $T_K^{orb}$ , which can be measured by resonant ultrasound spectroscopy, and a corresponding logarithmic divergence,  $\chi_s \sim \ln T$ , of the spin susceptibility below  $T_{K1}^{spin}$ . In addition, due to the series of MFLs that arise at  $T_K^{orb}$  and  $T_{K2}^{spin}$ , there would be a  $C_v \sim T \ln T$  behavior down to  $\Delta_{JT}^2/T_K^{orb}$ .

The applicability of our work to the iron-based SCs, especially the mechanisms for superconductivity, SDW and nematicity remain open issues for future work. However, we emphasize that the ‘‘Schrieffer effect’’ causes  $T_{Korb} \gg T_K^{spin}$ , and we believe the MFL behavior survives in a lattice, with FL behavior restored at a lower temperature due to breaking of tetrahedral symmetry or a phase transition to a broken symmetry state. We

suggest that critical orbital fluctuations within the  $e_g$  orbitals could provide a natural mechanism for nematic order, and the SDW state could arise from an RKKY instability in the dense limit[25]. Finally, it is known from studies of the over-screened single Kondo impurity[17] that there is a divergent susceptibility for composite SC pairing and it remains an interesting question as to whether any of these divergent susceptibilities play a role in the dense materials.

We gratefully acknowledge discussions with Natan Andrei, Gabriel Kotliar, Zlatko Tesanovic and Jan Zaanen on aspects of this work. This work is supported by DOE grant DE-FG02-99ER45790.

- 
- [1] Y. Kamihara, T. Watanabe, T. Hirano, and H. Hosono, *J. Am. Chem. Soc.* **130**, 3296 (2008).
  - [2] J.W. Lynn, and P. Dai *Physica C* **469**, 469 (2009).
  - [3] W.Z. Hu, *et. al.* *Phys. Rev. Lett.* **101**, 257005 (2008).
  - [4] D.N. Basov, *et. al.* *Nat. Phys.* **5**, 647 (2009).
  - [5] A. Tamai, *et. al.* *Phys. Rev. Lett.* **104**, 097002 (2010).
  - [6] Y. Xia, *et. al.* *Phys. Rev. Lett.* **103**, 037002 (2009).
  - [7] Q. Si, and E. Abrahams *Phys. Rev. Lett.* **101**, 076401 (2008).
  - [8] Z.P. Yin, K. Haule, and G. Kotliar *Nat. Phys.* **7**, 294 (2011).
  - [9] D. Basov, and A.V. Chubukov *Nat. Phys.* **7**, 272 (2011); P.J. Hirschfeld, M.M. Korshunov, and I.I. Mazin arXiv:1106.3712; D.J. Scalapino arXiv:1002.2413, and references therein.
  - [10] D.C. Johnston *Adv. Phys.* **59**, 803, (2010) and references therein.
  - [11] P. Dai, *et. al.* *Nature Mat.* **7**, 953 (2008).
  - [12] K. Yamada, *et. al.* *J. Phys. Soc. Jpn* **77**, 083704 (2008).
  - [13] M. Yamashita, *et. al.* arXiv:1103.0885
  - [14] S.K. Goh, *et. al.* *Phys. Rev. B* **82**, 094502 (2010).
  - [15] J.R. Schrieffer, *J. Appl. Phys.* **32**, 1143 (1967).
  - [16] A.H. Nevidomskyy, and P. Coleman *Phys. Rev. Lett.* **103**, 147205 (2009); P. Werner, E. Gull, M. Troyer, and A.J. Millis *Phys. Rev. Lett.* **101**, 166405 (2008); K. Haule, J.H. Shim, and G. Kotliar *Phys. Rev. Lett.* **100**, 226402 (2008)
  - [17] V.J. Emery, and S.A. Kivelson *Phys. Rev. B* **46**, 10812 (1992); V.J. Emery, and S.A. Kivelson, *Phys. Rev. Lett.* **71**, 3701 (1993).
  - [18] P. Coleman, L.B. Ioffe, and A.M. Tsvelik *Phys. Rev. B* **52**, 6611 (1995).
  - [19] J.M. Maldacena, and A.W.W. Ludwig *Nuc. Phys. B* **506**, 565 (1997).
  - [20] J. Gan, N. Andrei, and P. Coleman *Phys. Rev. Lett.* **70**, 686 (1993).
  - [21] Z. Qin, *et. al.* *Solid State Commun.* **150**, 768 (2010).
  - [22] K.I. Kugel, and D.I. Khomskii *Sov. Phys. Usp.* **25**, 231 (1982).
  - [23] K. Le Hur, P. Simon, and L. Borda *Phys. Rev. B.* **69**, 045326 (2004).
  - [24] M.D. Daybell, and W.A. Steyert *Rev. Mod. Phys.* **40**, 380 (1968).
  - [25] K. Ingersent, B.A. Jones, and J.W. Wilkins *Phys. Rev. Lett.* **69**, 2594 (1992).